



Breaking wave contribution to low grazing angle radar backscatter from the ocean surface

Paul A. Hwang,¹ Mark A. Sletten,¹ and Jakov V. Toporkov¹

Received 28 January 2008; revised 9 June 2008; accepted 26 June 2008; published 10 September 2008.

[1] The anomaly of radar sea spikes, defined here as the non-Bragg scattering events with backscattering cross-section of horizontal polarization exceeding that of the vertical polarization, has been associated with steep wave features possibly going through wave-breaking process, with or without whitecap manifestation. This property is exploited for using a dual polarized radar as a remote sensing breaking wave detector. Field data collected in the ocean covering wind speeds from 7 to 15 m/s, grazing angles from 1.4 to 5.5°, and with different levels of background swell influence are analyzed to quantify the radar cross-section and Doppler velocity from sea surfaces with and without wave breaking. Key results of the breaking effects are increasing significantly the Doppler velocity of both polarizations (about 50% faster), enhancing the horizontally polarized backscattering cross-section drastically (with 10–15 dB increase), and producing relatively small change in the vertically polarized cross-section (about 1–2 dB increase). The presence of swell (in the same direction of wind waves) reduces both the radar backscatter and the impact of breaking waves on radar return. By inference, the swell presence decreases the ocean surface roughness and breaking activity. These results are consistent with earlier in-situ surface wave measurements and our expectation of swell modification of breaking process due to interaction of short waves and the orbital velocity of long swell.

Citation: Hwang, P. A., M. A. Sletten, and J. V. Toporkov (2008), Breaking wave contribution to low grazing angle radar backscatter from the ocean surface, *J. Geophys. Res.*, 113, C09017, doi:10.1029/2008JC004752.

1. Introduction

[2] The intensity of radar backscatter from the ocean surface at low grazing angle is considerably stronger than that expected from theoretical computation, especially for the horizontal polarization. For wind speeds (at 10 m reference elevation), U , between 7 and 15 m/s, a difference of about 20 dB is typical between the measured normalized radar cross-section of horizontal polarization, σ_{HH} , and computation based on Bragg scattering formula at grazing angle $\theta_g = 5.5^\circ$ and more than 40 dB at $\theta_g = 1.4^\circ$ (see section 3.1). This level of difference is much larger than that can be explained by tilting modulation of Bragg roughness. Many non-Bragg scattering mechanisms attributable to wave breaking have been suggested to explain the strong radar returns or sea spikes [e.g., Wetzel, 1990; Trizna, 1991, 1997; Trizna and Carlson, 1996]. Other alternative mechanisms such as Bragg scattering from short scale bound waves modulated by intermediate scale surface waves have also been suggested to explain the large deviation from the conventional two-scale models for grazing angles between

10 and 70°; for lower grazing angles non-Bragg contributions (suggested to be possibly due to sea spray) still need to be added to the modeled cross-section [e.g., Plant, 1997, 2003]. The Doppler property of horizontal-transmit-horizontal-receive (HH) return is also found to be very different from the vertical-transmit-vertical-receive (VV) return [Pidgeon, 1968; Keller *et al.*, 1986]. There have been many published side-by-side comparisons of HH and VV images showing the contrast of sea spike features in the two polarizations [e.g., Trizna and Carlson, 1996; Trizna, 1997; Hwang *et al.*, 2008]. Field experiments have been carried out to confirm the correlation of sea spikes with wave breaking and to employ the sea spike properties for quantifying the properties of surface breaking waves [Lewis and Olin, 1980; Jessup *et al.*, 1990, 1991a, 1991b; Trizna, 1991, 1997; Trizna and Carlson, 1996; Liu *et al.*, 1998; Frasier *et al.*, 1998; Phillips *et al.*, 2001; Hwang *et al.*, 2008].

[3] The improved understanding of the wave-breaking process can in turn provide feedback to refine our understanding on the effect of surface wave breaking on radar backscatter from the ocean surface. For example, Trizna [1991] presents the probability distribution function (PDF, that is, the cumulated probability density function, pdf) of low grazing angle (1–8°) X-band horizontally polarized radar cross-sections collected in the ocean from two experiments. The first one is under fully developed sea in the open ocean with steady wind blowing for over a 4-day period,

¹Remote Sensing Division, Naval Research Laboratory, Washington, DC, USA.

and the second one is under changing winds with random young seas. He shows that the distribution of the cross-section can be described by one Weibull distribution at low wind condition and two Weibull distributions for moderate to high wind conditions. He suggests that the first Weibull distribution at lower radar return amplitudes represents the distributed roughness and the second Weibull distribution for the higher radar return amplitudes is associated with discrete scatterers. He further assumes that the high radar returns in the second Weibull distribution region are the sea spikes associated with surface wave crests, both breaking and nonbreaking. The effective mean sea spike radar cross-section is shown to be about 15 to 30 dB larger than the median cross-section over a range of wind speeds between 4 and 30 m/s. He also comments on the strong impact of swell on radar return, noticing that the correlation of radar return with wind speed improves significantly when a time lag of about 9 hours is introduced to the time series in the fully developed sea data group. *Trizna and Carlson* [1996] report dual polarized X-band measurements in the coastal environments of Bermuda and La Jolla under light to moderate winds and in the absence of long gravity waves. Images from the HH polarization show more discrete character while those from the VV polarization show more spatially homogeneous texture. They propose that the difference in the spatial texture reflects the difference in the scattering mechanisms for the two polarizations: evenly distributed Bragg scatter patches for VV and spiky scatter from small asymmetric bore features for HH. They also present a multipath illumination model and identify the bore features as small scale breakers of between 2 and 4 cm in height with crest widths between 24 and 48 cm.

[4] Here we present an analysis quantifying the breaking wave effects on the radar backscattering cross-section of both VV and HH polarizations. Wave breaking is considered to be likely to occur when the polarization ratio exceeds certain threshold. Taking advantage of the results from many earlier investigations of the sea spike properties [e.g., *Lewis and Olin*, 1980; *Lee et al.*, 1995, 1996; *Trizna*, 1991, 1997; *Trizna and Carlson*, 1996; *Frasier et al.*, 1998; *Liu et al.*, 1998; *Melief et al.*, 2006] and following an earlier analysis of the present data set for quantifying the distribution of length and velocity scales of breaking surface waves and comparison of radar sea spikes with ocean surface whitecaps, wave braking is defined as the non-Bragg events when the polarization ratio $R_{\sigma} = \sigma_{HH} / \sigma_{VV} > 0$ dB [*Hwang et al.*, 2008]. Section 2 gives a brief review of the data set and the result from the breaking wave analysis. In section 3, we describe the analysis of wave-breaking effects on radar returns. Using the polarization ratio criterion, the radar returns are sorted into “probably” nonbreaking and breaking categories. The magnitude of the cross-section and Doppler velocity in each category is calculated and the total contribution of the few but large breaking scatterers is quantified with the field data. The dependence of wave-breaking effects on wind speed and background swell conditions is also investigated. As cautioned by two anonymous reviewers, the separation of breaking and nonbreaking waves on the basis of whether the polarization ratio is greater than or less than one is probably a very approximate one. The breaking process is sufficiently complex that it produces effects that cannot be captured by the polarization

ratio alone. A discussion of the possible pitfalls is given at the end of section 3. Section 4 is a summary of results.

2. Field Experiment

[5] In 2006, NRL deployed a modified marine radar, an acoustic array, and an optical video camera on an offshore tower as part of a research program designed to develop a model for the acoustic noise generated by a spatially varying breaking wavefield. The tower (Station SPAG1 at 31.38°N, 80.57°W about 60 km offshore of the east coast of Georgia, local water depth 25 m; see http://www.ndbc.noaa.gov/station_page.php?station=SPAG1) is also designated as R2 of the South Atlantic Bight Synoptic Offshore Observational Network (SABSOON). The Station SPAG1 is instrumented with basic wind and wave sensors. Data available on the Web site mentioned above are the hourly wind direction, wind speed, wind gust, significant wave height, and air and water temperatures. Additional information of the peak wave period and surface wave spectrum is available from a nearby buoy 41008 (at 31.40°N, 80.87°W, 18 m depth) maintained by the National Data Buoy Center (NDBC), about 28.5 km to the west of SPAG1. One of the objectives of this program is to exploit the sea-spike/breaking-wave relationship by developing a low-grazing angle, dual-polarized, coherent radar as a breaking wave detector. The radar consists of a Raytheon Pathfinder magnetron transmitter with a center frequency of 9.3 GHz, two marine-radar-type fan beam antennas (one vertically polarized, the other horizontal), and a custom, coherent receiver. Pulse-to-pulse switching between the two antennas is used to collect HH and VV backscatter on alternate pulses at a per-polarization pulse repetition frequency (PRF) of up to 1200 Hz; for the data presented here, the PRF is 300 Hz. The azimuthal beam width of the antennas is 1.2° and the elevation beam width is 22°. The magnetron pulse width is approximately 50 ns, resulting in a range resolution of about 8 m. The acquisition program over-samples and the ground range resolution is 1.5 m in the received data. Peak transmitted power is approximately 1 kW. Postprocessing yields data of radar cross-section and Doppler velocity averaged into 1° bins. The range of the average grazing angle, θ_g , in the data set presented here is from 1.4 to 5.5°. The processed data length for each case is 340 s.

[6] Experimental data from three windy days in March and April 2006 were collected. All cases are under northerly wind events (within about 30° directional variations). The radar antennas are fixed on the northeastern corner of the tower pointing to the north and looking into the horizon so the radar waves propagate in the upwind direction of the wind-generated waves in all the data reported here. The data set has been analyzed for the properties of sea spikes attributable to surface wave breaking, and in turn, to use the sea spike information to investigate the properties of surface breaking waves [*Hwang et al.*, 2008]. Detailed description of the environmental conditions has been presented in that paper and a brief summary is given here for convenience. The wave conditions of the three days of radar data acquisition are all mixed seas. For 22 March 2006, a southerly wind event of up to about 19 m/s wind speed occurred a day before and built up waves reaching about 2 m height and 7 s period. The wind died down over a duration

Table 1. Relevant Environmental Conditions and Breaking Probability Derived From Sea Spike Analysis [Hwang et al., 2008]^a

U (m/s)	H_s (m)	T_p (s)	P_s (%)	#
12.9	1.4	3.6	7.86	1
12.9	1.8	4.1	8.61	2
12.9	1.8	4.2	8.21	3
12.1	1.5	4.7	6.28	4
10.5	1.4	4.6	7.53	5
9.8	1.3	4.5	7.29	6
8.9	1.3	4.5	5.79	7
8.2	1.3	4.8	3.43	8
6.9	1.2	4.6	4.40	9
13.0	2.1	5.9	6.93	10
14.5	2.3	5.7	6.39	11
14.4	2.4	5.8	5.28	12
13.7	2.7	6.1	5.51	13
12.9	2.7	5.7	5.88	14
12.7	2.6	5.9	5.72	15
11.3	2.1	5.7	6.14	16
10.7	2.0	5.5	4.78	17
10.5	2.0	5.4	5.05	18
13.0	2.3	5.5	7.94	19
12.0	2.2	5.9	7.40	20
12.0	2.5	6.7	6.27	21
10.7	2.3	6.6	4.82	22
10.0	2.3	6.5	3.73	23
10.0	2.4	7.1	5.08	24
10.0	2.3	6.7	5.63	25
10.0	2.3	6.5	5.21	26
10.0	2.3	6.1	3.36	27
10.0	2.1	6.0	6.53	28
9.2	2.1	7.5	6.73	29

^a#1–9, 22 March 2006; #10–18, 10 April 2006; #19–29, 11 April 2006.

of about 10 hours then reversed direction and a northerly wind of about 13 m/s prevailed at the beginning of the experiment. A new wind wave system developed over the mild adverse swell, the swell intensity in terms of wave height is mostly less than 0.2 m, calculated from the wave spectrum measured by the NDBC buoy [Hwang et al., 2008]. The significant wave height of this data group is between 1.2 and 1.8 m (Table 1, #1–9), so the swell is very mild in terms of the relative wave energy (proportional to wave height squared) and this data group can be considered as dominantly wind-generated sea. For 10 April 2006 and 11 April 2006, the wind direction remained steady from NNE the whole time. Wind speed varied about semidiurnally. This long and quasisteady wind episode started more than one day prior to radar data acquisition. The wave height continued to increase in the first half and then decreased in the second half of 10 April 2006 while wave period remained almost unchanged. For 11 April 2006, the wave period displayed a generally increasing trend the whole time while wave height was mostly constant at the first half and then slowly decreased in the second half. The complicated evolutions of the wave height and wave period are atypical of locally generated wind waves, pointing out the significant modification of the wavefield by the background swell in these two data groups. The wind speed, wave height and wave period at the radar data collection time are listed in Table 1, together with the breaking probability derived from the pdf of the polarization ratio.

[7] The main step of the data analysis involves the construction of the complex envelope of the received radar

signal, $V(t, r)$ using the Hilbert transform [e.g., Papoulis, 1991] of each radar pulse,

$$V(t, r) = a(t, r)e^{i\phi(t, r)}, \quad (1)$$

where t is time, r ground range, a amplitude and ϕ phase. The relative normalized cross-section is derived from the square of the amplitude taking into account the cubic range falloff,

$$\sigma(t, r) = C(r) \frac{a(t, r)^2}{r^3}, \quad (2)$$

where the factor C includes the antenna pattern provided by the manufacturer and an unknown calibration reference. The instantaneous Doppler frequency of surface scattering element is calculated by the temporal derivative of the unwrapped phase of the complex signal,

$$\omega_D(t, r) = \frac{\partial\phi(t, r)}{\partial t}. \quad (3)$$

This method is basically the covariance approach to spectral moment estimation from pulse pairs as described by Miller and Rochwarger [1972]. Thompson and Jansen [1993] also showed that the Doppler frequency derived from this approach is equivalent to the mean Doppler frequency calculated from the first moment of the Doppler spectrum (their equations (1)–(6)). To reduce data noise, a running average with a window of 50 temporal pixels is performed for σ and ω_D , yielding an equivalent integration time of 1/6 s (for the data presented here, the differential time is 1/300 s). Examples of the pdf of σ and ω_D for the total population and the breaking subpopulation are shown in Hwang et al. [2008, Figures 6 and 7, respectively].

[8] The breaking wave analysis of the radar returns shows that the distribution of breaking wave speed is narrow-banded with an average between 2.0 and 2.6 m/s in mixed seas for wind speeds between 7 and 15 m/s. The corresponding average breaking wavelength is between 2.5 and 4.3 m. The length or velocity scale of wave breaking is only weakly related to the length or velocity scale of the dominant wave. This observation reflects the local and discrete nature of the breaking process and may have significant implications on quantifying various breaking properties such as the energy dissipation, momentum flux or area of turnover by breaking waves. The fraction of sea spike coverage generally increases with wind speed but the trend of increase is modified by the intensity and relative direction of background swell. Similarities and differences between sea spikes and whitecaps are also investigated. In particular, while both quantities show a similar power law dependence on wind speed, the fraction of sea spike coverage is considerably higher than that of whitecap coverage. This result reflects the prevalence of steep features that produce non-Bragg facets and short-scale waves bounded to intermediate scale waves during breaking. These non-Bragg facets and bound waves contribute significantly to enhancing the radar sea return but may not entrain air to produce whitecap signature. Here we continue the analysis focusing on quantifying the effects of breaking

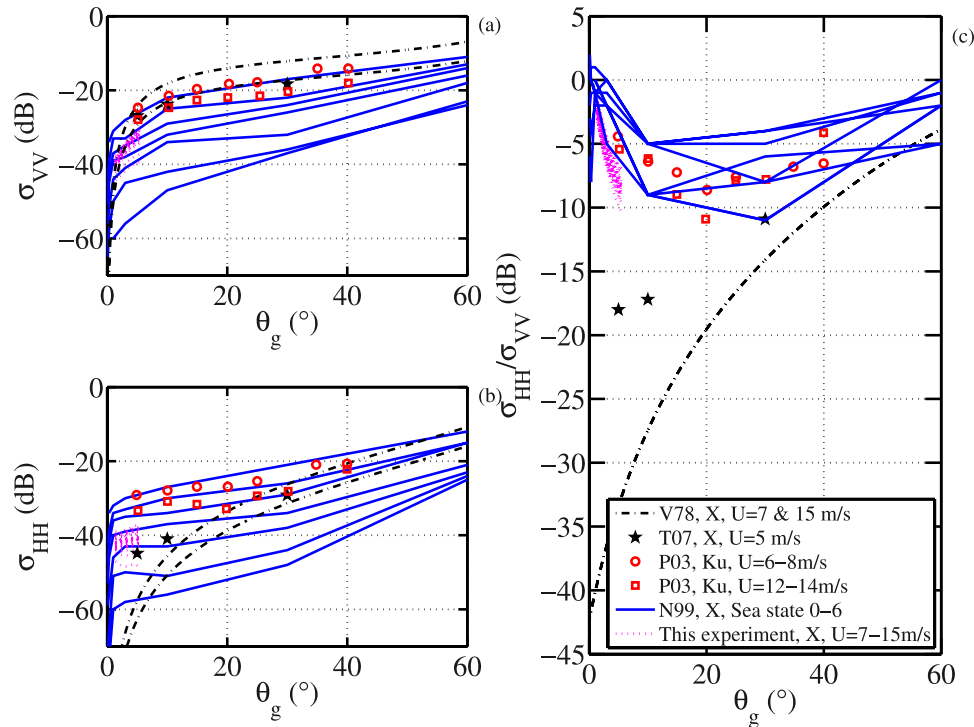


Figure 1. (a) σ_{VV} , (b) σ_{HH} and (c) R_σ as functions of the grazing angle. X-band: dotted curve, present study ($U = 7\text{--}15$ m/s); solid curve, Nathanson [1999], hydrographic sea states 0 to 6 (increasing upward); dashed-and-dotted curve, Bragg scattering calculation for $U = 7$ and 15 m/s [Valenzuela, 1978]; star, numerical calculation by Toporkov and Sletten [2007], $U = 5$ m/s; square and circle, Ku-band data of Plant [2003], $U = 6\text{--}8$ and 12–14 m/s, respectively.

waves on radar sea return by comparing the subpopulations of backscatter data with and without breaking-induced sea spikes.

3. Breaking Wave Contribution to Radar Backscatter

3.1. Data Set

[9] A brief summary of the environmental conditions of the full data set is given in Table 1. The wind speed varies from 7 to 15 m/s, wave height from 1.2 to 2.7 m, and peak wave period from 3.6 to 7.5 s. The wave conditions are dominantly mixed sea with different degrees of ocean swell presence. The least swell influence occurs in the reference data group 22 March 2006; the other two, 10 April 2006 and 11 April 2006, are under moderate swell modification. The dotted curves in Figures 1a and 1b show the scatterplot of the VV and HH relative normalized cross-sections, σ_{VV} and σ_{HH} , averaged in one-degree bins of the grazing angle, and Figure 1c shows the polarization ratio $R_\sigma = \sigma_{HH}/\sigma_{VV}$. Superimposed in the figure with solid lines are the experimental data (averaged over all wind directions with respect to the radar incidence) reported by Nathanson [1999, chapter 7]. The latter are tabulated for hydrographic sea states 0 to 6 [Nathanson, 1999, Figure 7.1] and several radar frequencies; only the X-band (9.3 GHz) data are shown (solid curves, sea state increases upward).

[10] As explained earlier, our radar was not field calibrated. The radar cross-section was computed with the relevant specifications provided by the manufacturer and accounted

for the cubic range falloff. We also measured the difference in the HH and VV transmission losses due to the difference in the cable lengths used for the two antennas and take this into account in the data processing. In Figure 1, we have shifted our data to be close to the curves corresponding to sea states 3 to 5 of the Nathanson data collection. Also shown in the figure are two dashed curves calculated for Bragg scattering contribution at 7 and 15 m/s wind speeds using the formula by Valenzuela [1978]. Finally, the results based on two-dimensional direct numerical simulations by Toporkov and Sletten [2007] at $U = 5$ m/s and $\theta_g = 5, 10$ and 30° are shown as stars. Significant differences between theoretical or numerical simulations with field measurements are obvious. Particularly, the σ_{HH} is substantially enhanced at low grazing angle in the field data and the trend of R_σ as a function of grazing angle is reversed between measurements and computations. The much larger computed Bragg scattering cross-section of vertical polarization in comparison to field data (Figure 1a) may suggest the difficulty of specifying the surface wave spectrum of short ocean waves in the Bragg resonance length scale of the X-band radar waves; the Elfouhaily spectral model [Elfouhaily et al., 1997] is used here.

[11] The wind-speed or sea-state dependence of the polarization ratio is somewhat less systematic as compared to that of the cross-sections. For the field data, the polarization ratio increases toward low grazing angle. This trend is opposite to that expected from Bragg scattering computation and the radar return at higher grazing angles (Figure 1c). The magnitude of R_σ is also much larger in the experimental

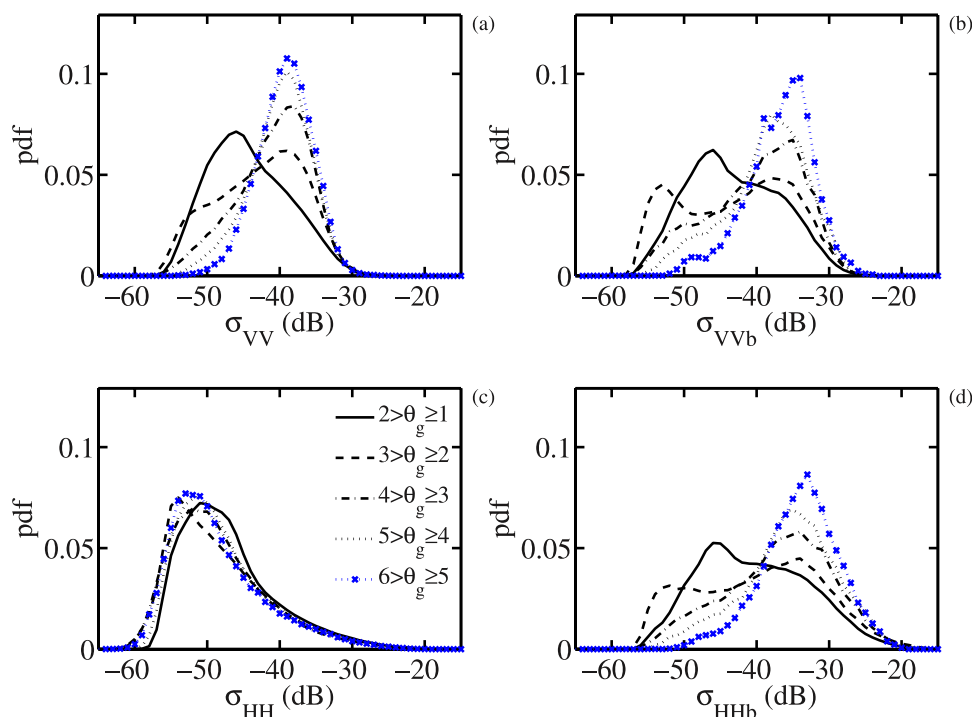


Figure 2. The pdf of the relative normalized cross-section in 1° grazing angle bins. Upper row is VV, lower row is HH; left column is for all population, right column is for breaking subpopulation ($R_\sigma > 0$ dB).

data in comparison to the theoretical calculation; the difference is from about 25 dB at $\theta_g = 5^\circ$ to 40 dB at $\theta_g = 1^\circ$. This deviation from Bragg scattering mechanism (including two-scale models) is also found in other radar frequencies. An example is shown in the figure with the Ku-band (14 GHz) tower data (6–8 and 12–14 m/s, squares and circles, respectively) reported by *Plant* [2003]. Similar results are also reported for L-band (1.238 GHz) returns by *Forget et al.* [2006, Figure 16].

[12] In the present analysis, probable wave-breaking events are identified with the criterion of polarization ratio $R_\sigma = \sigma_{HH}/\sigma_{VV} > 0$ dB, based on earlier analyses of low grazing angle radar backscatter data in the ocean and comparison with whitecap coverage on the ocean surface [e.g., *Lee et al.*, 1995, 1996; *Frasier et al.*, 1998; *Liu et al.*, 1998; *Phillips et al.*, 2001; *Melief et al.*, 2006; *Hwang et al.*, 2008]. The breaking wave contribution to radar backscatter from the ocean surface is evaluated from comparing the statistical properties of radar backscatter with and without sea spike events attributable to surface wave breaking. The population of the scattering cross-sections is divided into three major categories: the total population, nonbreaking subpopulation ($R_\sigma < -2$ dB, the variables are distinguished by a subscript n), and breaking subpopulation ($R_\sigma > 0$ dB, distinguished by a subscript b). Several notable results on the backscattering cross-section and the Doppler velocity are described in the following.

3.2. Backscattering Cross-Section

[13] While the pdf of σ_{VV} and σ_{HH} are considerably different, those of the breaking subpopulations, σ_{VVb} and σ_{HHb} , are essentially similar (Figure 2, wind speed 6.9 m/s; see also Figure 7 of *Hwang et al.* [2008] for a higher wind

speed case, 13 m/s). This may suggest that specular, double-bounce and other non-Bragg mechanisms play an important role in radar backscatter at low grazing angle.

[14] Figures 3a and 3b show the average VV and HH cross-sections, respectively, of probably breaking and non-breaking subpopulations for $\theta_g = 1.4$ and 5.5° . The effect of wave breaking on σ_{VV} is relatively small, the difference with and without breaking is generally within about 1 dB at $\theta_g = 5.5^\circ$ and 2 dB at $\theta_g = 1.4^\circ$ (the connected symbols represent the reference data group 22 March 2006, to be further discussed below). The impact of breaking on σ_{HH} is substantial, about 15 dB at $\theta_g = 5.5^\circ$ and 10 dB at $\theta_g = 1.4^\circ$. Table 2 presents the ensemble average of σ_{VV} and σ_{HH} of the three different categories (total population, breaking and nonbreaking subpopulations) at five different grazing angles. The effect of breaking on backscattering cross-section can be evaluated from comparing the entries of σ_{VVb} (breaking) and σ_{VVn} (nonbreaking), and σ_{HHb} and σ_{HHn} . The breaking effect also appears in the dependence of the scattering cross-section on the grazing angle. In the total and nonbreaking categories, about 7.5 dB drop is found in σ_{VV} and σ_{VVn} for grazing angles from 5.5° to 1.4° and 1.5 to 2.8 dB drop in σ_{HH} and σ_{HHn} . For the breaking category, both σ_{VVb} and σ_{HHb} have a similar 6 dB drop in the same grazing angle range. (The standard deviation of the various cross-section statistics listed above ranges from 1.2 to 2.4 dB.) The ensemble average R_σ for the three categories are also listed in Table 2, showing relatively invariant of the polarization ratio of the breaking returns with respect to the grazing angle (within 0.5 dB average) while a 6.4-dB change occurs in the polarization ratio of the total population and 4.5 dB in the nonbreaking subpopulation. These results may reflect the shadowing effects on low grazing

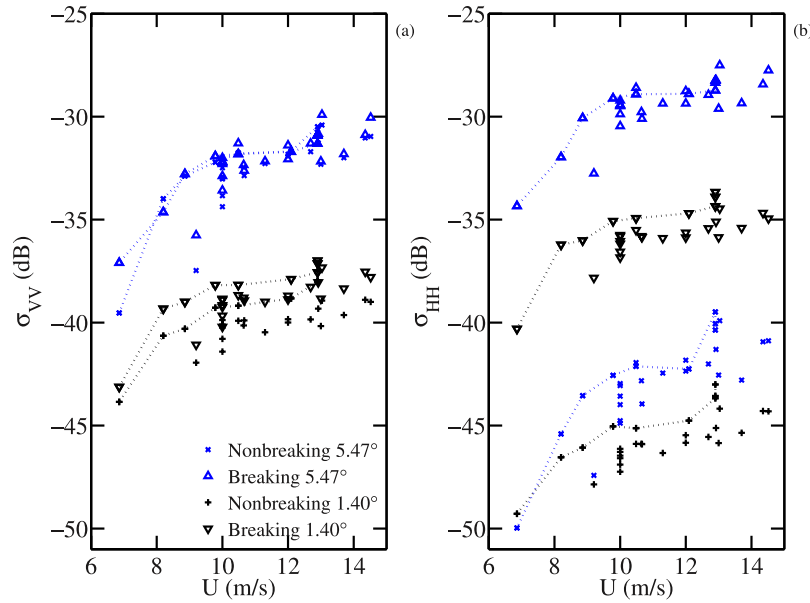


Figure 3. Average cross-sections of nonbreaking and breaking subpopulations at two grazing angles plotted against wind speed, (a) vertical polarization and (b) horizontal polarization.

angle radar backscatter. The effect of shadowing increases toward lower grazing angle. Because wave breaking primarily occurs at the crest phase of the waveform, quantities (cross-section and Doppler velocity) associated with sea spikes due to wave breaking would be least impacted by the shadowing effect, as reflected in the weaker grazing angle dependence in comparison to that of the quantities of nonbreaking subpopulation or total population.

[15] As discussed by *Hwang et al.* [2008] and summarized in the last section, the environmental condition of 22 March 2006 resembles closest to local wind-generated seas. The data points are shown with connected symbols in Figure 3. They form an approximate upper bound of the total data set in both breaking and nonbreaking categories, suggesting that the presence of swell reduces in general the radar backscatter from the ocean and lessens the variation of the radar backscatter. By inference, the swell reduces ocean surface roughness and wave breaking, which is one of the conclusions reached from analysis of in-situ measured intermediate- and short-scale surface waves. These short- and intermediate-scale waves were measured using high-resolution wave gauges mounted on a free-drifting platform to alleviate the complication of Doppler frequency shift on the interpretation of the wave number spectrum derived from the time series measurements [*Hwang and Wang*, 2004; *Hwang*, 2005, 2007]. Further discussions of the swell effects are deferred to section 3.4.

[16] The net effect of breaking waves on the radar cross-section can be assessed from comparing the cross-sections of the total population and the nonbreaking subpopulation. As shown in Figure 4, the net impact on σ_{VV} is small (about $\pm 10\%$ in our data set covering wind speeds between 7 and 15 m/s and θ_g from 1.4 to 5.5°). In contrast, the contribution of breaking (from less than 10% of the total population, Table 1) for σ_{HH} is on the same level as or larger than that from the majority of the nonbreaking sea surface area. The sea spike contribution in σ_{HH} shows an increasing trend

toward higher wind speed. The wind speed dependence becomes stronger at lower grazing angle; the slope of the linear trend on wind speed is about 0.05 and 0.1 at $\theta_g = 5.5^\circ$ and 1.4°, respectively (Figure 4). The observed wind speed dependence can be attributed to the positive correlation between breaking occurrence and wind speed. Shadowing effect, again, may play a role in the observed grazing angle dependence of the rate of increase with wind speed. As wind speed increases, wind waves become steeper, increasing the degree of shadowing and amplifying the relative effect of wave breaking on the radar return signal.

3.3. Doppler Velocity

[17] The average Doppler velocity, u_D , of backscatter is consistently higher in HH (u_{DH}) than in VV (u_{DV}) as first noticed by *Pidgeon* [1968] from his analysis of the C-band

Table 2. Ensemble Average of the Cross-Section and Doppler Velocity of the Total Population and Breaking and Nonbreaking Subpopulations

Average	Grazing Angle, θ_g (°)				
θ_g (°)	1.39	2.43	3.45	4.46	5.47
σ_{VV} (dB)	-40.06	-37.32	-35.14	-33.63	-32.51
σ_{VVb} (dB)	-38.74	-37.31	-35.03	-33.48	-32.16
σ_{VVn} (dB)	-39.87	-36.92	-35.00	-33.59	-32.56
σ_{HH} (dB)	-42.50	-42.09	-41.51	-41.15	-40.99
σ_{HHb} (dB)	-35.68	-34.10	-31.82	-30.51	-29.48
σ_{HHn} (dB)	-45.67	-44.63	-43.84	-43.19	-42.83
R_σ (dB)	-2.44	-4.77	-6.38	-7.52	-8.49
R_{rb} (dB)	3.07	3.21	3.21	2.98	2.68
R_{rn} (dB)	-5.81	-7.71	-8.84	-9.60	-10.28
u_{DV} (m/s)	1.85	1.61	1.50	1.44	1.41
u_{DVb} (m/s)	2.10	2.02	1.99	1.97	1.97
u_{DVn} (m/s)	1.66	1.45	1.37	1.33	1.32
u_{DH} (m/s)	2.25	2.09	1.98	1.91	1.85
u_{DHb} (m/s)	2.48	2.45	2.43	2.41	2.41
u_{DHn} (m/s)	2.11	1.95	1.86	1.81	1.76

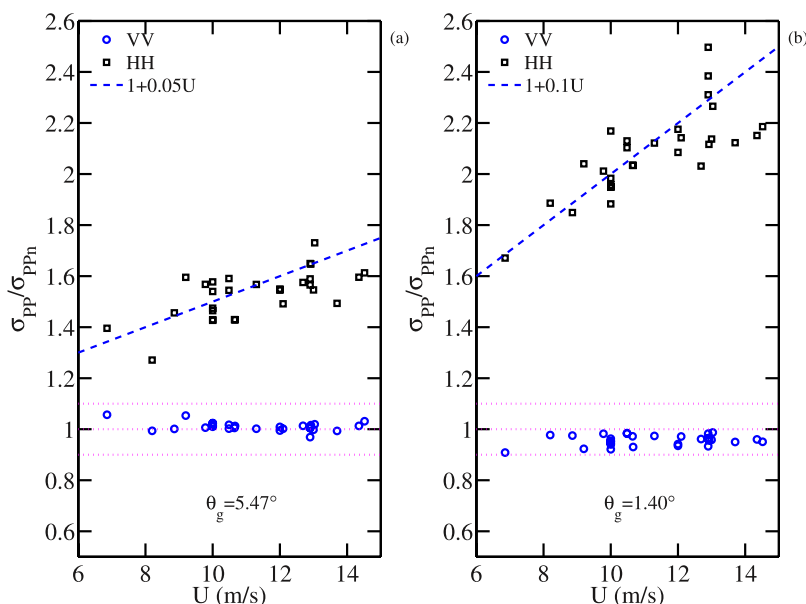


Figure 4. Net effect of breaking on the cross-section in terms of the ratio between the backscattering cross sections of total population and nonbreaking subpopulation, (a) $\theta_g = 5.5^\circ$ and (b) $\theta_g = 1.4^\circ$.

data (5.7 GHz). He commented that the Doppler shift is independent of the grazing angle. This statement seems to be in contradiction to some of his own data shown in his Figure 7, in which the results with three different pulse lengths (0.3, 1 and 3 μ s) for the condition of 13 m/s wind and 1-m wave height are displayed. The 1- μ s cases cover the widest range of grazing angles ($1-3^\circ$) in that figure, and a trend of increasing u_D toward lower grazing angle is conspicuous. Examples of the dependence of Doppler velocity on grazing angle in our measurements are shown in Figure 5a for $U = 6.9$ and 12.9 m/s. For the wind speed

dependence, Figure 5b shows u_{DH} and u_{DV} from the present measurements for $\theta_g = 1.4^\circ$ together with Pidgeon's data as summarized in Figure 7.9 of Nathanson [1999]. The range of wind speeds in Pidgeon's experiment is much broader in HH than VV data. The rate of change of his HH data seems to have a sharp change near U at about 5 to 7 m/s. The rate of increase of the (HH) Doppler velocity with wind in the lower wind region is much larger than that in the higher wind region. The Doppler velocity difference ($u_{DH} - u_{DV}$) is between 0.5 and 1 m/s.

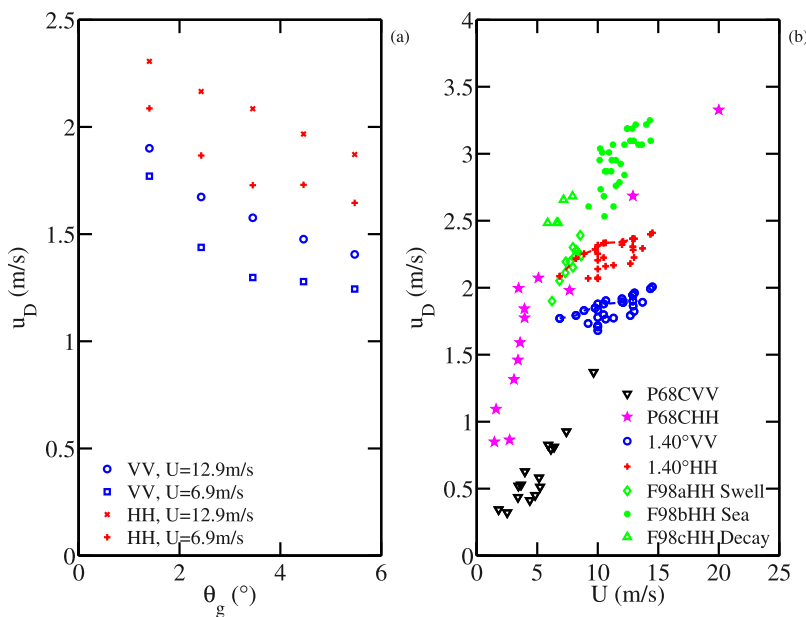


Figure 5. (a) Examples of the grazing angle dependence of the Doppler velocity; two wind speeds are shown. (b) Doppler velocity data from the present experiment and other sources [Pidgeon, 1968; Frasier et al., 1998]; see discussion in the text.

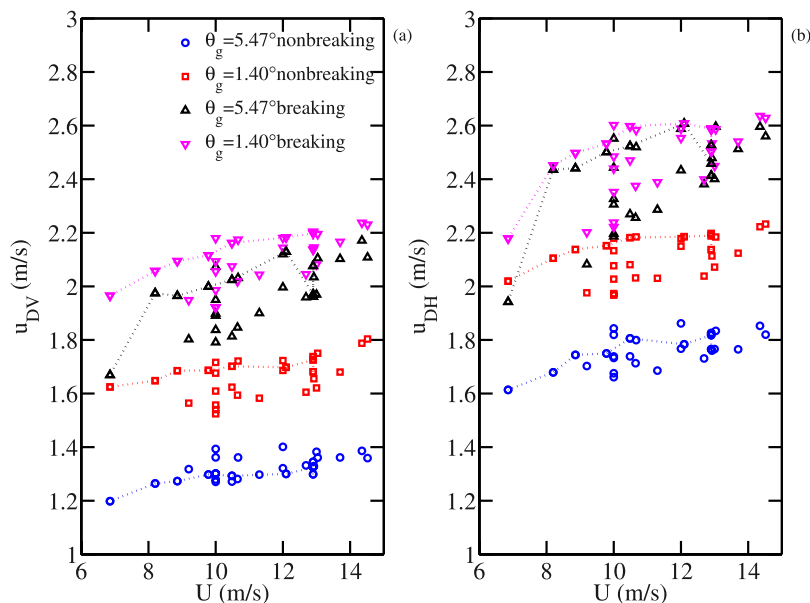


Figure 6. Comparison of the average Doppler velocity of breaking and nonbreaking subpopulations at two different grazing angles, (a) vertical polarization and (b) horizontal polarization.

[18] In our experiment with wind speeds from 7 to 15 m/s, both u_{DH} and u_{DV} show an increasing trend toward higher wind speed and lower grazing angle and u_{DH} is larger than u_{DV} by about 0.5 m/s. The rate of increase with wind speed in our data is somewhat less than that of Pidgeon's in the overlapped wind conditions. Also shown in this figure are the data of radar sea spike "event speed" obtained from spatiotemporal feature tracking reported by *Frasier et al.* [1998]. They compared the event speed with the mean speed of breaking waves defined as the normalized integrated product of the phase speed and acceleration spectrum derived from the Doppler velocity spectrum (their equation (3)) and found that the two velocity scales are more or less proportional to each other (their Figure 12). Although the event speed is different from the mean Doppler velocity discussed here, the variation with wind speed of the two breaking velocity scales is somewhat similar but the data scatter is rather large. Some of the data scatter is probably caused by the swell condition. In the experiment of *Frasier et al.* [1998], the Doppler velocity under the conditions identified as swell dominant (shown with the diamond symbol in Figure 5) is considerably smaller than that under the developing and decaying wind sea conditions. In the present experiment, the wave conditions are mixed seas with wind-sea dominant. The effect of decreasing Doppler velocity with increasing swell influence is also apparent (in Figure 5, the reference data set of 22 March 2006 with most wind-sea domination is shown with connected symbols.) The description of wind and wave conditions in the work of *Pidgeon* [1968] is much less extensive and it is difficult to assess the swell influence in his data. As a concluding remark of Figure 5, it is emphasized that different definitions of the mean Doppler velocity have been used in the three data groups cited. It is not clear how much of the observed difference is attributable to the different definitions of the velocity scale.

[19] Figure 6 shows the mean Doppler velocities of non-breaking and breaking subpopulations as a function of wind speed for two grazing angles. The nonbreaking Doppler velocity displays a strong grazing angle dependence, while the breaking Doppler velocity shows less variation. This again may be attributed to the shadowing effect, which has the least impact near the crest region of the waveform where wave breaking generally take place. The Doppler velocity of breaking scatterers is considerably larger than that of the nonbreaking ones for both polarizations; the difference, $Du_D = u_{Db} - u_{Dn}$, is about 0.7 to 0.8 m/s at $\theta_g = 5.5^\circ$ and about 0.4 to 0.5 m/s at $\theta_g = 1.4^\circ$ as the upper bounds for $U > 8$ m/s (Figure 7). These differences are a substantial fraction of the mean Doppler velocity of the nonbreaking subpopulation, between 1.2 and 1.8 m/s for VV and 1.6 to 2.2 m/s for HH. For reference, Table 2 lists the ensemble average of the Doppler velocity of three categories (total, breaking, and nonbreaking) at five difference grazing angles. There is an appreciable trend of increasing Doppler velocity toward low grazing angle in both polarizations of total population and nonbreaking subpopulation. The dependence of the Doppler velocity on grazing angle is almost diminished in the breaking subpopulation. The wind speed dependence of the Doppler velocity difference between the breaking and nonbreaking scatterers is relatively mild in the present data set, especially for $U > 8$ m/s (Figure 7). In mixed sea conditions, increasing swell intensity tends to decrease the Doppler velocity difference; the data of 22 March 2006 (least swell influence, connected symbols) represent an approximate upper bound of the data clusters. Further discussion of the swell effect is given in section 3.4.

[20] While the Doppler velocity of breaking scatterers is considerably higher than that of the nonbreaking ones, the net effect on the resulting average Doppler velocity of the total population is mitigated by the small fraction of the breaking waves (less than 10% in our data set, Table 1). Figure 8 shows discernable difference in the mean Doppler

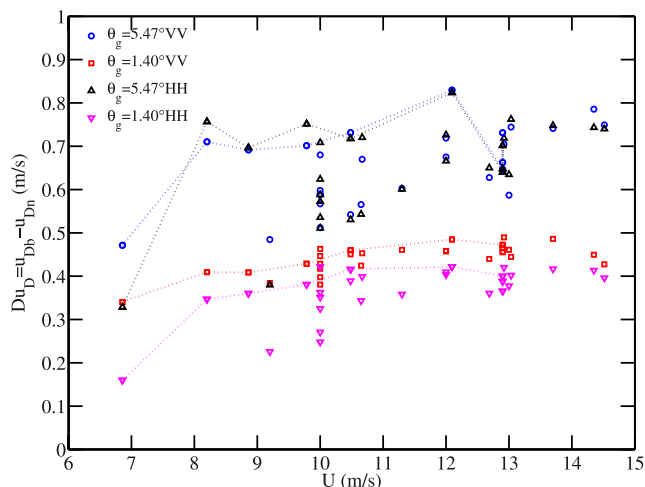


Figure 7. Difference of the average Doppler velocity between breaking and nonbreaking subpopulations as a function of wind speed for two different grazing angles.

velocities of the total population and the nonbreaking subpopulation ($\Delta u_D = u_D - u_{Dn}$) in VV and HH returns. The difference is in fact larger in VV than HH, this is especially significant since the Doppler velocity of the vertical return is relatively slower. Comparing the net effects of wave breaking on the scattering cross-section (Figure 4) and the Doppler velocity (Figure 8), it suggests that while a reasonably accurate VV cross-section may be obtained when the breaking contribution (due to whatever mechanisms) is neglected, the VV Doppler velocity would be considerably in error if the breaking contribution is ignored. For HH scattering, explicit inclusion of the breaking contribution is critical to an accurate prediction of both cross-section and Doppler velocity.

3.4. Mixed Sea Effect on Wave Breaking

[21] As commented earlier, the data group 22 March 2006 (connected symbols in Figures 3 and 5–10) is frequently separated from the other two groups (10 April 2006 and 11 April 2006). In particular, they seem to form an approximate upper bound of the backscattering cross-section and the Doppler velocity measurements for both VV and HH polarizations. As noted earlier, the environmental condition of 22 March 2006 is that of locally wind-generated waves superimposed on a mild counter swell (a reversed wind event after a previous wind event died down). For the other two groups (10 April 2006 and 11 April 2006), the wind field had been steady for more than 24 hours and remained steady for the entire two days of radar data collection; the wave properties were characterized by local wind waves superimposed on swell in the same direction. Wave-breaking process can be modulated by the background current in a significant way due to wave-current interaction [Phillips and Banner, 1974; Banner and Phillips, 1974; Phillips, 1977]. In essence, the modulation effect of the background wave orbital motion causes the small waves riding on the orbital current to undergo breaking prematurely (that is, before reaching the geometrically unstable condition that limits the wave growth). The length scales of the breaking waves (both wave height and wavelength) with background wave modulation become smaller than the corresponding breaking length scales in the absence of swell modulation due to interruption of wind wave growth by premature wave breaking. Figures 9a and 9b show the average cross-section and Doppler velocity of the horizontally polarized breaking subpopulation. Assuming that the spectral density of the surface waves is proportional to the cross-section and that the breaking wavelength is related to the breaking phase speed through the dispersion relation [see discussions in Frasier et al., 1998; Phillips et al., 2001; Hwang et al., 2008], the deduced breaking wave spectral density and wavelength are shown in Figures 9c and 9d. Again, the

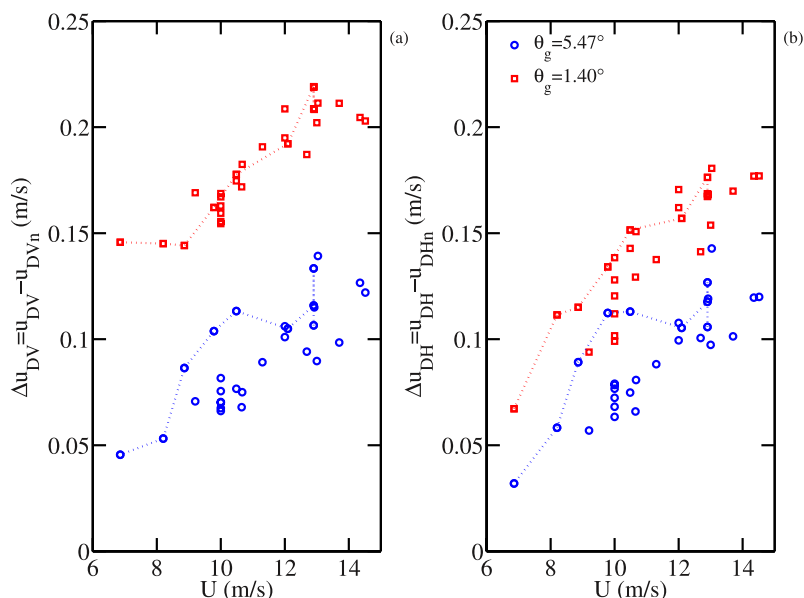


Figure 8. Net effect of breaking on the Doppler velocity; (a) vertical polarization and (b) horizontal polarization.

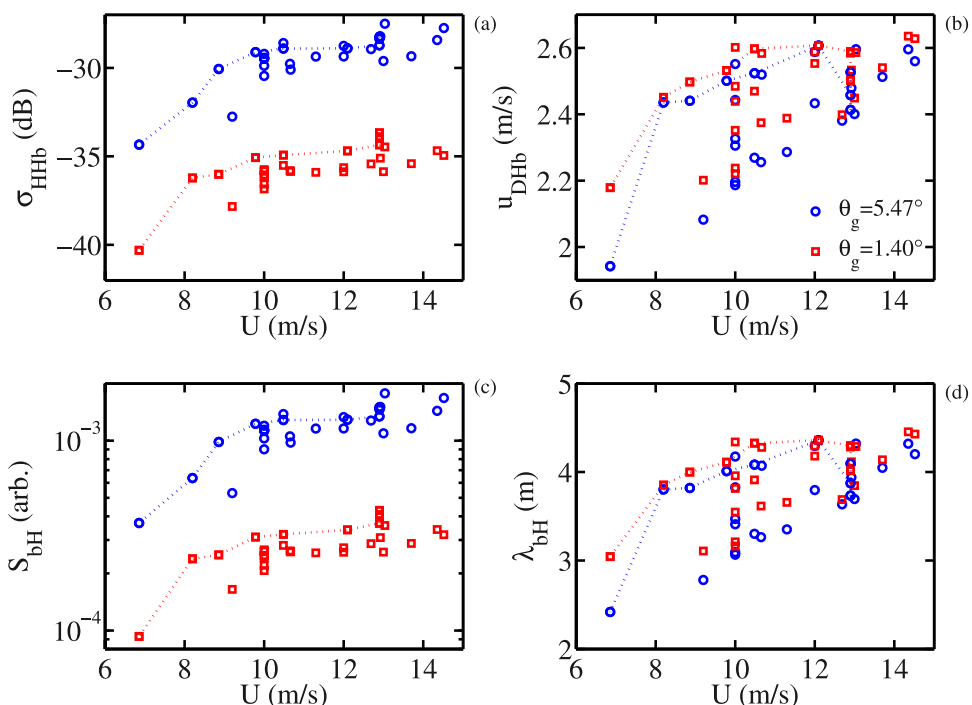


Figure 9. (a) Average cross-section and (b) Doppler velocity of the breaking subpopulation; and the deduced (c) spectral density (proportional to a scale dependent on the grazing angle) and (d) breaking wavelength of the breaking waves. All quantities are from horizontal polarization data.

dotted lines connect the data of 22 March 2006, and the result suggests that in the presence of moderate background swell (data of 10 April 2006 and 11 April 2006, non-connected symbols), the breaking wave height and wave-

length are reduced. Similar result of swell reducing the breaking velocity scale is also found in the data of *Frasier et al.* [1998]. Figure 5 displays their Doppler velocity data separated into three categories: dominated by swell, active

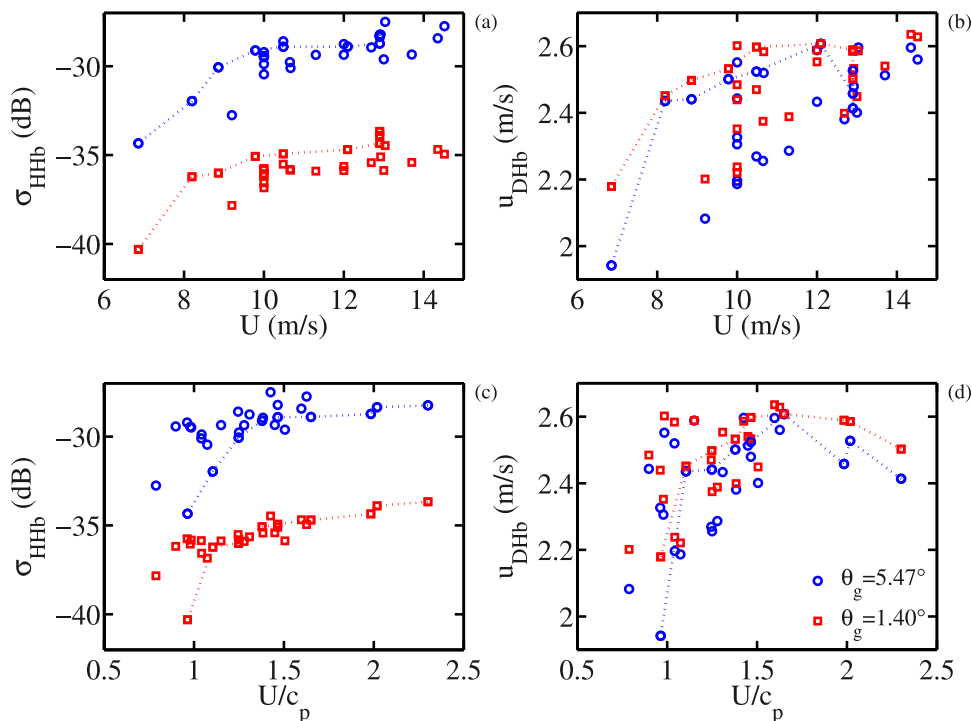


Figure 10. (a and b) Same as Figure 9a and b. (c and d) The corresponding data presented with U/c_p as an indicator of swell influence.

developing sea, and decaying sea. The Doppler velocity in the category of swell-dominated condition is clearly smaller than that of the other two categories.

[22] In a discussion of breaking wavelength from the analysis of wave dissipation function using wave data measured by high resolution capacitance wave gauges mounted on a free drifting platform, *Hwang and Wang* [2004] found that the length scale of the dissipation function is narrowly distributed, the peak of the distribution function shifts from 1.6-m wavelength in wind sea to a broader region between 0.3 and 0.6 m in mixed seas. The measured length scale of breaking waves can vary considerably depending on the sensing technique. *Hwang* [2007] presents a more detailed discussion of the breaking length scale analyses based on acoustic, radar and wave gauge measurements (see his Figure 4). Despite this difficulty for inter-comparison between different data sets, the decreasing breaking length scale with increasing swell influence is a consistent feature in all the data sets examined.

[23] Presently, we do not have a good way of defining the parameters for quantifying the swell effects on air–sea interaction processes such as wind-wave growth, ocean surface drag coefficient or wave breaking because there are so many factors involved. Several prominent ones include the relative wavelength, wave height, propagation direction, frequency bandwidth, . . . , between locally generated wind-waves and nonlocal swell. One of the parameters frequently used to quantify mixed seas is the ratio of wind speed and peak wave phase speed, U/c_p . The presence of swell tends to increase the characteristic phase speed of the wavefield, thus under the same wind condition, the stronger swell influence would shift data points toward lower U/c_p . Figure 10 compares the dependence on U (top) and U/c_p (below) of the HH cross-section and Doppler velocity of the breaking subpopulation. The prominent feature in the latter presentation is the increased data scatter toward small U/c_p , which is an indication of increased swell influence in the present context. The physical interpretations of these two presentations (U and U/c_p) are quite different. In the former, the data indicate that breaking wave height and wavelength are reduced by the influence of swell; in the later, the modulation of swell amplifies the range of the breaking wavelength scales (both wave height and wavelength) thus increasing the data scatter toward larger swell influence (smaller U/c_p).

3.5. Discussion

[24] As pointed out by two anonymous reviewers, the separation of breaking and nonbreaking waves on the basis of whether the polarization ratio is greater than or less than one is probably a very approximate one. The breaking process is sufficiently complex that it produces effects that cannot be captured by the polarization ratio alone. It is entirely possible to have breaking wave effects that do not lead to polarization ratios greater than one [*Plant*, 1997; *Plant et al.*, 1999]. Therefore it is highly likely that the “nonbreaking” parts of the backscatter in this paper in fact contain some breaking wave effects that show up in HH more than VV. This would help explain the much larger nonbreaking Doppler velocities at HH than at VV (by about 50 cm/s!) as well as the quite large HH/VV polarization ratios compared to Bragg scattering, and the surprisingly

small reduction in nonbreaking HH cross-section from 5.5 to 1.4° grazing. It would also help explain why at very low grazing the difference between the total Doppler velocity and that for nonbreaking waves increases so much at very low grazing angles: when VV Bragg finally falls to the level of breaking backscatter, the mean Doppler shift increases. The increase in Doppler shift would not be so obvious in HH backscatter because some breaking waves are already included in what is called nonbreaking.

4. Summary

[25] Wave breaking is an important ocean surface process that plays many critical roles in air–sea interaction, gas transfer, generation and entrainment of turbulence and bubble plume, and creation of geometric features that cause significant enhancement of radar backscatter over a broad range of radar frequencies. Although the frequency of occurrence and the area of coverage of breaking waves are small (both are less than about 10% for wind speed lower than 15 m/s, see Table 1 and whitecap coverage discussions in *Hwang and Sletten* [2008]), the backscattering cross-section of the breaking scatterers is about one to two orders of magnitude larger than that of the nonbreaking scatterers for the horizontal polarization (Figure 3b). The net contribution to the average cross-section from the small fraction of breaking scatterers is about the same magnitude as that from the remaining nonbreaking scatterers (more than 90% of the total population). For the vertical polarization, the net impact of breaking waves on the backscattering cross-section is very small (Figure 4). While the effect of wave breaking on the backscattering cross-section is considerably different for VV and HH, its impact on the Doppler velocity is very similar for the two polarizations. The upper bound of the difference between the Doppler velocities of breaking and nonbreaking scatterers is about 0.8 m/s at $\theta_g = 5.5^\circ$ and about 0.5 m/s at $\theta_g = 1.4^\circ$ (Figure 7). The Doppler velocity difference of breaking and nonbreaking scatterers shows a mild increasing trend with the wind velocity and its magnitude is decreased with increasing swell influence. Weighted with the breaking probability, the net increase in the Doppler velocity is about 0.05 to 0.2 m/s at $\theta_g = 5.5^\circ$ and about 0.05 to 0.15 m/s at $\theta_g = 1.4^\circ$ (Figure 8). Somewhat surprisingly, the effect of breaking on Doppler velocity is stronger for VV than HH. Comparing Figures 4 and 8 on the net effects of breaking on cross-section and Doppler velocity, respectively, it is noted that while the breaking influence can be ignored in the computation of the VV cross-section, its impacts on the Doppler velocity of both polarizations as well as the HH cross-section are significant.

[26] Although the environmental conditions encountered in the present data set are limited in scope, the results show a conspicuous feature of wind sea data serving as the upper bounds of the data clusters of backscattering cross-section and Doppler velocity. This feature is also persistent in the subpopulation of breaking scatterers only. An inference of this observation is that the swell presence decreases the ocean surface roughness and breaking activity. The result is consistent with the radar data presented by *Frasier et al.* [1998], the in-situ measurements of the ocean surface roughness [*Hwang and Wang*, 2004; *Hwang*, 2005, 2007]

and our expectation of the modification of wave-breaking process by the orbital velocity of background waves [Phillips and Banner, 1974; Banner and Phillips, 1974; Phillips, 1977]. Under this mechanism, breaking occurs prematurely with the presence of swell and the development of small and intermediate scale waves is interrupted, resulting in reduced spectral density and wavelength of the braking waves in comparison with those under the reference wind sea condition in the absence of swell. The radar measurements of breaking scatterers under different degrees of swell influence reflect the expected change of breaking process due to swell influence (Figures 9 and 10).

[27] **Acknowledgments.** We are grateful to the insightful comments from two anonymous reviewers. This work is sponsored by the Office of Naval Research (NRL work units 8027 and 8953 and program element 61153N; NRL contribution number NRL/JA/7260-08-0035).

References

- Banner, M. L., and O. M. Phillips (1974), On the incipient breaking of small scale waves, *J. Fluid Mech.*, *65*, 647–656.
- Elfouhaily, T., B. Chapron, K. Katsaros, and D. Vandemark (1997), A unified directional spectrum for long and short wind-driven waves, *J. Geophys. Res.*, *102*, 15,781–15,796.
- Forget, P., M. Saillard, and P. Broche (2006), Observations of the sea surface by coherent L band radar at low grazing angles in a nearshore environment, *J. Geophys. Res.*, *111*, C09015, doi:10.1029/2005JC002900.
- Frasier, S. J., Y. Liu, and R. E. McIntosh (1998), Space-time properties of radar sea spikes and their relation to wind and wave conditions, *J. Geophys. Res.*, *103*, 18,745–18,757.
- Hwang, P. A. (2005), Wave number spectrum and mean-square slope of intermediate-scale ocean surface waves, *J. Geophys. Res.*, *110*, C10029, doi:10.1029/2005JC003002.
- Hwang, P. A. (2007), Spectral signature of wave breaking in surface wave components of intermediate length scale, *J. Mar. Sys.*, *66*, 28–37.
- Hwang, P. A., and M. A. Sletten (2008), Energy dissipation of wind-generated waves and whitecap coverage, *J. Geophys. Res.*, *113*, C02012, doi:10.1029/2007JC004277.
- Hwang, P. A., and D. W. Wang (2004), An empirical investigation of source term balance of small scale surface waves, *Geophys. Res. Lett.*, *31*, L15301, doi:10.1029/2004GL020080.
- Hwang, P. A., M. A. Sletten, and J. V. Toporkov (2008), Analysis of radar sea return for breaking wave investigation, *J. Geophys. Res.*, *113*, C02003, doi:10.1029/2007JC004319.
- Jessup, A., W. Keller, and W. Melville (1990), Measurements of sea spikes in microwave backscatter at moderate incidence, *J. Geophys. Res.*, *95*, 9679–9688.
- Jessup, A., W. Melville, and W. Keller (1991a), Breaking waves affect microwave backscatter: 1. Dependence on wind and wave conditions, *J. Geophys. Res.*, *96*, 20,547–20,559.
- Jessup, A., W. Melville, and W. Keller (1991b), Breaking waves affect microwave backscatter: 2. Detection and verification, *J. Geophys. Res.*, *96*, 20,561–20,569.
- Keller, W., W. Plant, and G. Valenzuela (1986), Observations of breaking ocean waves with coherent microwave radar, in *Wave Dynamics and Radio Probing of the Sea Surface*, edited by O. M. Phillips and K. Hasselmann, Plenum, New York.
- Lee, P. H. Y., J. D. Barter, K. L. Beach, C. L. Hindman, B. M. Lake, H. Rungaldier, J. C. Shelton, A. B. Williams, R. Yee, and H. C. Yuen (1995), X band microwave backscattering from ocean waves, *J. Geophys. Res.*, *100*, 2591–2611.
- Lee, P. H. Y., J. D. Barter, E. Caponi, M. Caponi, C. L. Hindman, B. M. Lake, and H. Rungaldier (1996), Wind-speed dependence of small-grazing-angle microwave backscatter from sea surfaces, *IEEE Trans. Antennas Propag.*, *44*, 333–340.
- Lewis, B., and I. Olin (1980), Experimental study and theoretical model of high resolution radar backscatter from the sea, *Radio Sci.*, *15*, 815–828.
- Liu, Y., S. J. Frasier, and R. E. McIntosh (1998), Measurement and classification of low-grazing-angle radar sea spikes, *IEEE Trans. Antenna Propag.*, *46*, 27–40.
- Melief, H. W., H. Greidanus, P. van Genderen, and P. Hoozeboom (2006), Analysis of sea spikes in radar sea clutter data, *IEEE Trans. Geosci. Remote Sens.*, *44*, 985–993.
- Miller, K. S., and M. M. Rochwarger (1972), A covariance approach to spectral moment estimation, *IEEE Trans. Inform. Theory*, 588–596.
- Nathanson, F. E. (1999), *Radar Design Principles*, 2nd ed., 720 pp., Scitech Publ., Inc., Mendham, New Jersey.
- Papoulis, A. (1991), *Probability, Random Variables, and Stochastic Processes*, 3rd ed., McGraw-Hill, Inc., New York.
- Phillips, O. M. (1977), *The Dynamics of the Upper Ocean*, 2nd ed., 336 pp., Cambridge Univ. Press, New York.
- Phillips, O. M., and M. L. Banner (1974), Wave breaking in the presence of wind drift and swell, *J. Fluid Mech.*, *66*, 625–640.
- Phillips, O. M., F. L. Posner, and J. P. Hansen (2001), High range resolution radar measurements of the speed distribution of breaking events in wind generated ocean waves: Surface impulse and wave energy dissipation rates, *J. Phys. Oceanogr.*, *31*, 450–460.
- Pidgeon, V. W. (1968), Doppler dependence of radar sea return, *J. Geophys. Res.*, *73*, 1333–1341.
- Plant, W. J. (1997), A model for microwave Doppler sea return at high incidence angles: Bragg scattering from bound, tilted waves, *J. Geophys. Res.*, *102*, 21,131–21,146.
- Plant, W. J. (2003), Microwave sea return at moderate to high incidence angles, *Wave Random Media*, *13*, 339–354.
- Plant, W. J., P. H. Dahl, and W. C. Keller (1999), Microwave and acoustic scattering from parasitic capillary waves, *J. Geophys. Res.*, *104*, 25,853–25,866.
- Thompson, D. R., and J. R. Jensen (1993), Synthetic aperture radar interferometry applied to ship generated internal waves in the 1989 Loch Linnhe Experiment, *J. Geophys. Res.*, *98*, 10,259–10,269.
- Toporkov, J. V., and M. A. Sletten (2007), Statistical properties of low grazing range resolved sea surface backscatter generated through two dimensional direct numerical simulations, *IEEE Trans. Geosci. Remote Sens.*, *45*, 1181–1197.
- Trizna, D. B. (1991), Statistics of low grazing angle radar sea scatter for moderate and fully developed ocean waves, *IEEE Trans. Antennas Propag.*, *39*, 1681–1690.
- Trizna, D. B. (1997), A model for Brewster angle damping and multipath effects on the microwave radar sea echo at low grazing angle, *IEEE Trans. Geosci. Remote Sens.*, *35*, 1232–1244.
- Trizna, D. B., and D. J. Carlson (1996), Studies of dual polarized low grazing angle radar sea scatter in nearshore regions, *IEEE Trans. Geosci. Remote Sens.*, *34*, 747–757.
- Valenzuela, G. R. (1978), Theories for the interaction of electromagnetic and ocean waves a review, *Bound. Layer Meteorol.*, *13*, 61–85.
- Wetzel, L. B., (1990), Electromagnetic scattering from the sea at low grazing angles, in *Surface Waves and Fluxes*, 2, edited by G. L. Geernaert and W. J. Plant, pp. 109–171, Kluwer Academic Publ., New York.

P. A. Hwang, M. A. Sletten, and J. V. Toporkov, Remote Sensing Division, Naval Research Laboratory, 4555 Overlook Avenue SW, Washington, DC 20375, USA. (paul.hwang@nrl.navy.mil; mark.sletton@nrl.navy.mil; jakov.toporkov@nrl.navy.mil)